Cell Reports
Physical Science

CellPress
OPEN ACCESS

Article

Scalable bacterial production of moldable and recyclable biomineralized cellulose with tunable mechanical properties

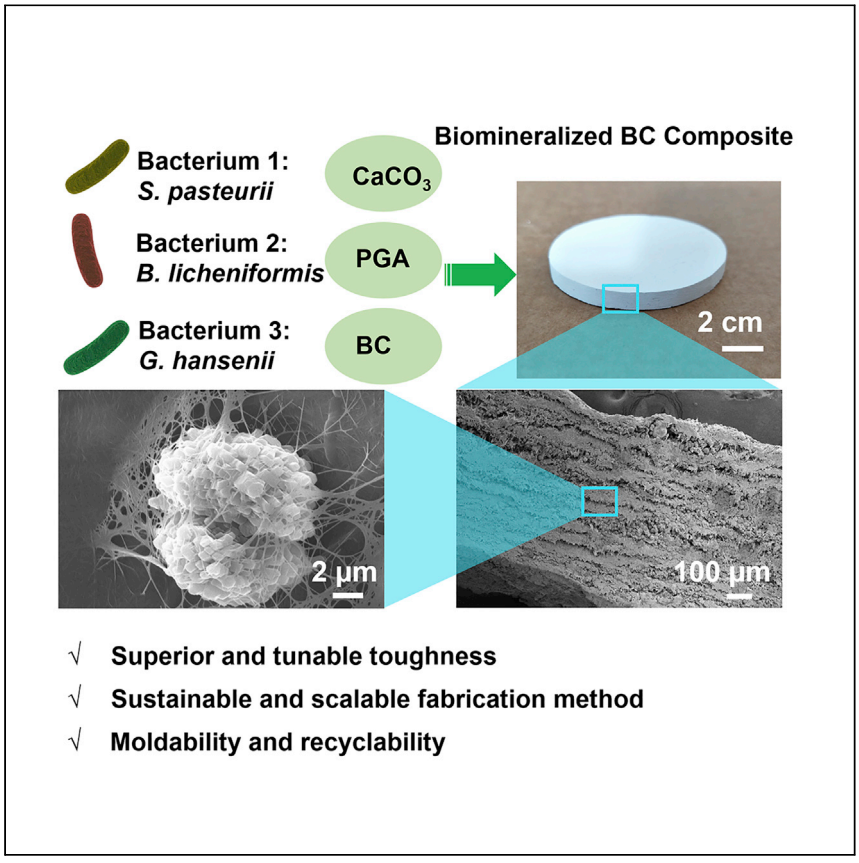

Scalable and biological production of nacre-like high-performance materials remains challenging. Yu et al. produce a self-assembling 3D moldable material with a layered microstructure. The material shows high toughness values, making it suitable for use in protective garments and plastics substitution.

Kui Yu, Ewa M. Spiesz, Srikkanth Balasubramanian, Dominik T. Schmieden, Anne S. Meyer, Marie-Eve Aubin-Tam

m.e.aubin-tam@tudelft.nl

Highlights

Nacre-like cellulose-based composite materials are fully produced by bacteria

The composites are moldable, biodegradable, and recyclable

A toughness of 22 MJ m^{-3} with 60% inorganic content is achieved

The material shows high compressibility and impact resistance

Yu et al., Cell Reports Physical Science 2, 100464
June 23, 2021
https://doi.org/10.1016/j.xcrp.2021.100464

Cell Reports
Physical Science

CellPress
OPEN ACCESS

Article

Scalable bacterial production of moldable and recyclable biomineralized cellulose with tunable mechanical properties

Kui Yu,[1] Ewa M. Spiesz,[1] Srikkanth Balasubramanian,[1] Dominik T. Schmieden,[1] Anne S. Meyer,[2] and Marie-Eve Aubin-Tam[1,3,*]

SUMMARY

Sustainable structural materials with excellent impact-resistance properties are urgently needed but challenging to produce, especially in a scalable fashion and with control over 3D shape. Here, we show that bacterial cellulose (BC) and bacterially precipitated calcium carbonate self-assemble into a layered structure reminiscent of tough biomineralized materials in nature (nacre, bone, dentin). The fabrication method consists of biomineralizing BC to form an organic/inorganic mixed slurry, in which calcium carbonate crystal size is controlled with bacterial poly(γ-glutamic acid) and magnesium ions. This slurry self-assembles into a layered material that combines high toughness and high impact and fire resistance. The rapid fabrication is readily scalable, without involving toxic chemicals. Notably, the biomineralized BC can be repeatedly recycled and molded into any desired 3D shape and size using a simple kitchen blender and sieve. This fully biodegradable composite is well suited for use as a component in daily life, including furniture, helmets, and protective garments.

INTRODUCTION

Petroleum-based high-performance structural materials play a vital role in the aerospace, biomedical, construction, and automotive industries due to their low cost, excellent mechanical properties, and large production scale.[1–3] However, the manufacture and usage of such materials cause multiple irreversible damage to the environment, including accumulation of plastic waste, chemical pollution, energy wastage, and climate change.[2] To reduce these negative effects on the planet, recyclable structural materials fabricated in a "green" manner are highly demanded.[4] The most abundant biodegradable polymer on earth, cellulose, draws high levels of attention as a raw material for the production of structural materials.[5] In general, plant-derived cellulose containing impurities such as lignin is used despite the fact that it requires an environmentally unfriendly delignification process to obtain cellulose nanofibers.[6] In contrast, bacterial cellulose (BC) has gained attention in recent years due to its high purity, which is obtained with sustainable processing conditions.[7,8] BC is an extracellular biopolymer secreted by certain microorganisms in the form of a hydrogel-like pellicle at the air-liquid interface.[9] The multiple advantages of BC, including its nanofibrous microstructure, light weight, low cost, biocompatibility, and biodegradability, make it an ideal candidate for producing the next generation of structural materials.[10] However, pure BC is brittle because of its high crystallinity. Even though BC possesses good tensile strength, its toughness is not sufficient for several applications with impact-resistance requirements

[1]Department of Bionanoscience, Kavli Institute of Nanoscience, Delft University of Technology, Van der Maasweg 9, 2629 HZ Delft, the Netherlands

[2]Department of Biology, University of Rochester, Rochester, NY 14627, USA

[3]Lead contact

*Correspondence: m.e.aubin-tam@tudelft.nl

https://doi.org/10.1016/j.xcrp.2021.100464

(e.g., helmets, protective garments). Also, pure BC is an organic material, which is less fire resistant compared to inorganic materials, limiting its range of applications.

To acquire BC-based materials with a combination of high tensile strength and toughness, which are often mutually exclusive,[11] several *in situ* and *ex situ* methods, including wet drawing,[12] wet spinning,[13] twisting,[14] and tape peeling,[15] have been developed. However, most of these methods focus on the production of one-dimensional (1D) fibers[16] or 2D films,[9] while 3D BC bulk materials are rarely reported. This difficulty in producing 3D materials based on BC on a large scale is mainly due to BC losing >99% of its weight upon drying, resulting in thin films with thicknesses from several centimeters to <0.1 mm (Figure S1). More recently, a 3D BC bulk material[10] was developed by adhering multiple BC layers and polymers together using a hot-pressing technique. However, high numbers of BC layers are needed to obtain the final 3D BC composites, and the hot-pressing process is highly energy consuming, which would greatly increase the material and energy costs during industrial-scale production.

To lower the material costs, tune the fire resistance and mechanical properties (e.g., stiffness, strength, toughness), and achieve the fabrication of 3D BC bulk composites, we combine BC with calcium carbonate ($CaCO_3$).[17] $CaCO_3$ is one of the most abundant inorganic raw materials in nature and is widely used in high-performance bioinspired structural materials.[18–22] While the preparation of $CaCO_3$-containing composites is easily realized with a mineralization method wherein $CaCO_3$ crystals are grown gradually on a supportive matrix,[18] the mineralization of BC remains challenging. Due to the dense structure and abundance of hydrogen bonding within BC networks, inorganic $CaCO_3$ crystals cannot easily penetrate and enter into the bulk BC hydrogel matrix[22] without the assistance of an external force.[18,23] Producing a highly mineralized BC (containing >50 wt% of $CaCO_3$) via the direct mineralization of bulk BC without external force requires weeks and months of repeated work, while the resulting material still does not possess competitive mechanical properties,[23] let alone large-scale production.[24] Organizing mineralized BC into an ordered bulk material with homogeneous inorganic crystal distribution and competitive mechanical properties remains a challenge and is of critical importance in developing BC-based 3D structural materials.

Here, we develop a hierarchical self-assembly approach to produce large-scale, shape- and size-controlled biomineralized BC composites with tunable mechanical properties, following an easy and industrially scalable protocol (Figure 1). Three different types of bacteria are used to produce the components that make up this composite. Bulk BC hydrogels are mechanically disintegrated into a fibrous suspension, followed by bacterially induced $CaCO_3$ biomineralization[25–27] to form an inorganic-organic mixed slurry. The crystal size and distribution can be adjusted by another bacterially produced biopolymer: poly(γ-glutamic acid) (PGA).[28] The bacterial slurry can then self-assemble into a material with a layered microstructure, achieving a toughness of 22 MJ m^{-3}, which is >5-fold higher than that of pure BC. The resultant layered structure of $CaCO_3$ separated by organic polymers (BC and PGA) is reminiscent of the hierarchical structures of tough biomineralized materials found in nature, such as nacre,[29] bone,[4] or dentin.[30] The homogeneous distribution of inorganic crystals together with the extensive crystal-fiber connections within the BC matrix enable the formation of stiff and tough 3D materials. This bacterially produced composite can be molded into different geometries, is recyclable, and shows promise for use in applications such as furniture and protective garments.

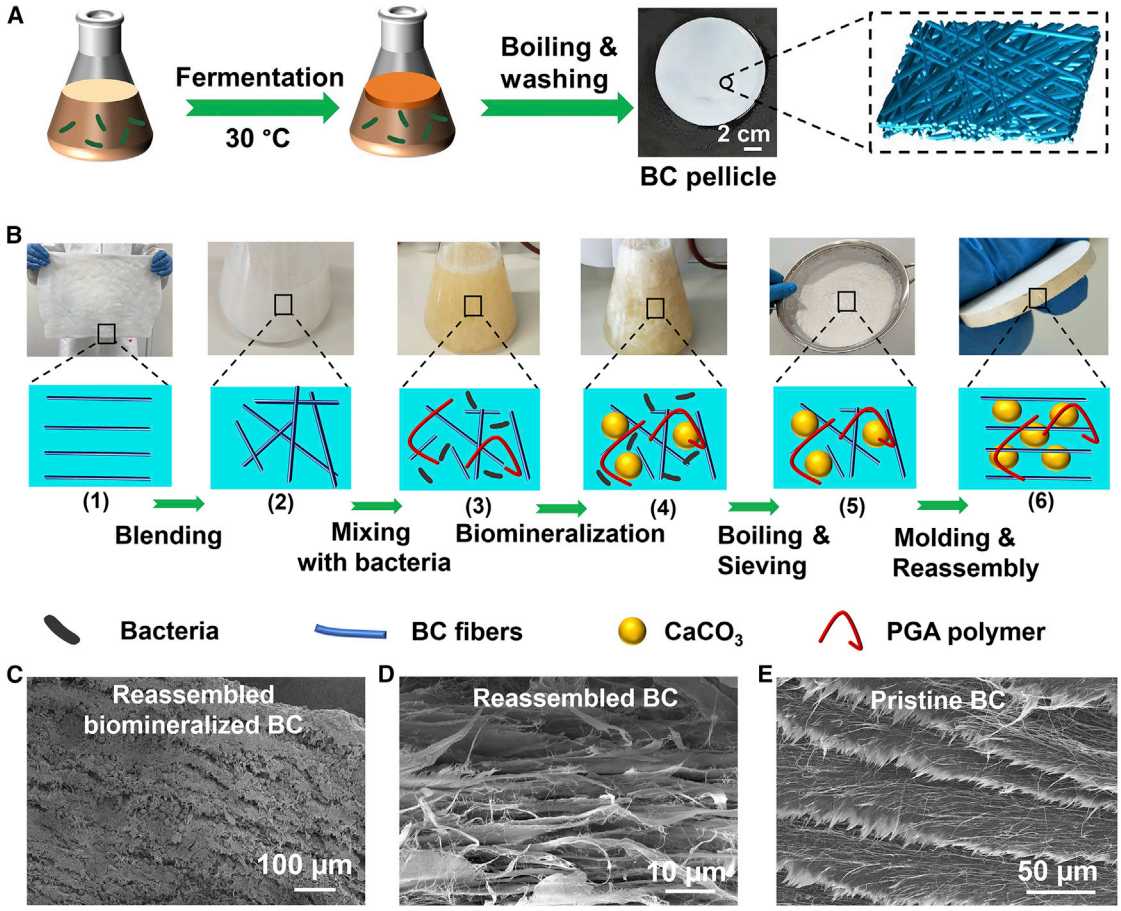

Figure 1. Biomineralized bacterial cellulose (BC) fabrication

(A) Fabrication procedure of BC, including a static *in situ* fermentation at 30°C, boiling with sodium hydroxide, and washing with distilled water. The BC pellicle shows a hydrogel-like appearance and a nano-fibrous layered microstructure.

(B) Fabrication procedure of the biomineralized BC, from step (1) to (6): (1)–(2) blending the BC hydrogel into a fibrous suspension, (2)–(3) mixing the BC fibrous suspension with the bacteria mineralization ingredients ($CaCl_2$, urea, bacteria, medium, and PGA), (3)–(4) biomineralization, (4)–(5) boiling and sieving the biomineralized slurry to remove the bacteria and medium, (5)–(6) molding the purified biomineralized BC slurry and solvent-evaporation-induced self-assembly. The final material shown on the picture was polished with sandpaper.

(C–E) Scanning electron microscopy (SEM) images of the cross-sections of (C) reassembled biomineralized BC composite, (D) reassembled BC, and (E) pristine BC.

RESULTS

Biological production and morphology of biomineralized BC

To achieve the environmentally friendly and scalable fabrication of BC-biomineralized 3D structural materials with excellent mechanical properties, a bacterially induced $CaCO_3$ biomineralization method[31,32] was used in combination with a solvent-evaporation-induced self-assembly method (Figure 1). BC was produced by microbial fermentation with a cellulose-producing strain, *Gluconacetobacter hansenii*.[33] After 2 weeks of growth, a wet BC pellicle was formed at the air-liquid interface (Figure 1A). This material was boiled with 1 w/v% sodium hydroxide solution and washed with water to remove impurities. To increase the degree of mineralization of the BC, the BC network was mechanically disintegrated (Figure 1B), so that the contact interface area between $CaCO_3$ and BC would be greatly increased during mineralization. For biomineralization, the disintegrated BC fibers were mixed in a bacterial growth medium containing *Sporosarcina pasteurii*, urea, and 10 mM calcium chloride ($CaCl_2$) (Figure S2). *S. pasteurii* secrete the enzyme urease, which

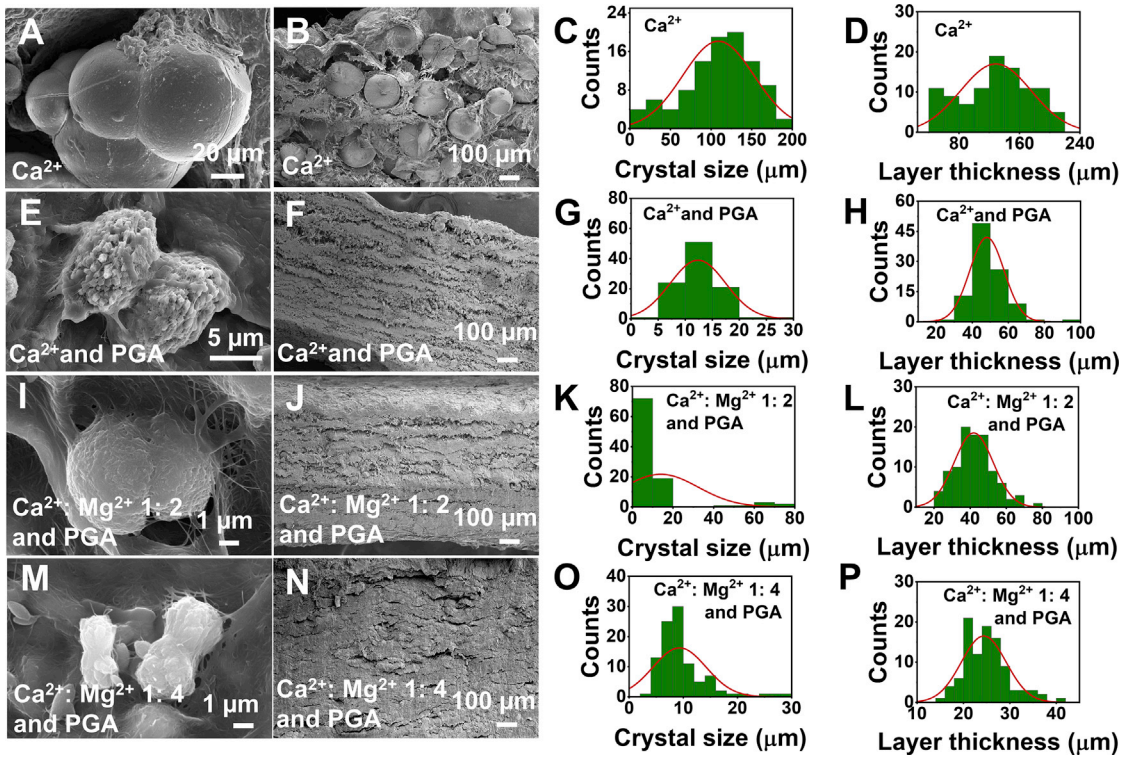

Figure 2. Morphology of biomineralized BC composites

(A, E, I, M) Representative SEM images of crystals within the biomineralized BC with (C, G, K, O) associated crystal size distributions.

(B, F, J, N) SEM images of the material cross-sections and (D, H, L, P) layer thickness distributions of biomineralized BC composites.

Biomineralized BC samples were fabricated either (A–D) without or (E–P) with PGA in the biomineralization medium and with either (A–H) only Ca^{2+}, or with a Ca^{2+}:Mg^{2+} ratio of (I–L) 1:2 or (M–P) 1:4 in the biomineralization medium. Data are represented as means ± SDs.

cleaves urea into ammonia and CO_3^{2-}, resulting in a pH increase and the formation of $CaCO_3$ crystals.[17] During this biomineralization procedure, the BC fibers were dispersed in the liquid and thus were able to be highly mineralized (Figure 1B). This biomineralized BC slurry was then purified by boiling on a heating plate for sterilization, washing with water to remove the unreacted residuals and the medium, and finally air drying. Thermal gravimetric analysis (TGA) showed 60 wt% $CaCO_3$ content in these samples (Figure S3).

After the biomineralization and the purification steps, we used scanning electron microscopy (SEM) to assess the microstructure of the air-dried biomineralized BC/$CaCO_3$ slurry. Remarkably, we observed that BC could reassemble into a layered structure, with $CaCO_3$ crystals entrapped within the layers (Figures 1C, 2A, and 2B). Due to the high aspect ratio of BC fibrils, pure BC suspensions formed by mechanical disintegration reassembled into a layered structure after drying (Figure 1D), similar to that of pristine BC (Figure 1E), as previously observed.[34,35] Therefore, our biomineralized BC composite likely adopted a layered structure because of this ability of the BC fibrous suspension to self-assemble.

SEM imaging of these samples revealed large $CaCO_3$ crystals (110 ± 40 μm crystal size) (Figures 2A and 2C) and a nonuniform cross-sectional layered morphology (Figure 2B) with a layer thickness of 130 ± 50 μm (Figure 2D). The relatively broad distribution in layer thickness (Figure 2D) is likely attributable to the broad crystal size distribution (Figure 2C) and large crystal size (Figure 2A).

We then attempted to obtain a more homogeneous layer distribution by reducing the $CaCO_3$ crystal sizes. Also, the presence of large crystals are likely to lead to stress concentrations[36] in certain structural features of the material and result in poor overall mechanical properties of the material.[37] To reduce the crystal size and in turn the layer thickness, chemically produced poly(acrylic acid) can be incorporated into the biomineralization medium, as the abundant carboxyl groups can act as binding sites for crystal growth and regulate the crystal size distribution.[38] Here, instead of poly(-acrylic acid), which is produced with the use of toxic chemicals,[39] we incorporated a similar polymer that can be bacterially produced, PGA.[28] PGA is a water-soluble, renewable polyamide polymer[40] produced by *Bacillus licheniformis*. PGA displays abundant carboxyl groups on its molecular backbone[41] that can provide binding sites for calcium ions (Ca^{2+}) during $CaCO_3$ mineralization.[42] When PGA was added to the medium for bacterial biomineralization, both the crystal size (12 $\pm$ 5 μm) (Figures 2E and 2G) and the layer thickness (48 $\pm$ 10 μm) (Figures 2F and 2H) were significantly reduced compared to samples without PGA in the biomineralization medium (Figures 2A–2D) ($p < 0.01$). We therefore conclude that the addition of PGA helps to form a layered structure with thinner and more narrowly distributed layer thicknesses, which is important for constructing layered bioinspired materials.[4] Therefore, unless indicated otherwise, the rest of the biomineralization procedures in this study were carried out in the presence of PGA.

To further reduce the crystal size, the formulation of biomineralization medium needed to be further optimized. In traditional chemical mineralization approaches, magnesium ions (Mg^{2+}) can be introduced to regulate the crystal size and morphology, as they inhibit the growth of $CaCO_3$ crystals.[43] We therefore added Mg^{2+} into the bacterial biomineralization system. Varying the Ca^{2+}:Mg^{2+} molar ratio in the biomineralization medium, while keeping the same overall ion concentration of 10 mM, resulted in different crystal sizes and morphologies (Figures 2I and 2M). With a Ca^{2+}:Mg^{2+} ratio of 1:2 in the biomineralization medium, the crystal diameter was 15 $\pm$ 19 μm (Figures 2I and 2K), while with a Ca^{2+}:Mg^{2+} ratio of 1:4, the crystal diameter dropped to 9.3 $\pm$ 4.9 μm (Figures 2M and 2O). Notably, the samples with both Ca^{2+} and Mg^{2+} assembled into a finely layered structure with a layer thickness of 42 $\pm$ 11 μm when the Ca^{2+}:Mg^{2+} ratio was 1:2 (Figures 2J and 2L), and 24 $\pm$ 5 μm when the Ca^{2+}:Mg^{2+} ratio was 1:4 (Figures 2N and 2P). X-ray diffraction (XRD) indicated that the $CaCO_3$ crystals in the biomineralized BC composites (Ca:Mg 1:4 with PGA) adopted a calcite polymorph[44] (Figure S4).

In summary, the layered structure of our material derives from the reassembly of BC fibers upon drying. After biomineralization, BC fibers are entangled with $CaCO_3$ crystals. During the drying procedure, BC fibers tend to aggregate together due to hydrogen bonding interactions through which $CaCO_3$ crystals can be entrapped into the reassembled BC network. The addition of PGA and Mg^{2+} can regulate the biomineralization procedure via inhibition of the crystal growth[43,45] and reduce the crystal diameter, which reduces the final layer thickness of our material.

Furthermore, the layered biomineralized BC composites (Ca^{2+}:Mg^{2+} 1:4) could be produced at large scale (Figure 3A; material diameter of 30 cm) and repeatedly deconstructed and molded into a wide variety of desired shapes (Figure 3B). The material recycle procedure was achieved by immersing the biomineralized BC material into water for 2 days. The softened biomineralized BC, together with water, was then re-blended with a simple kitchen blender into a slurry again. The slurry and water mixture was poured into a sieve, transferred into a mold of the desired shape, and air-dried to self-assemble into another biomineralized BC material. One single molded composite was able to be re-molded many times.

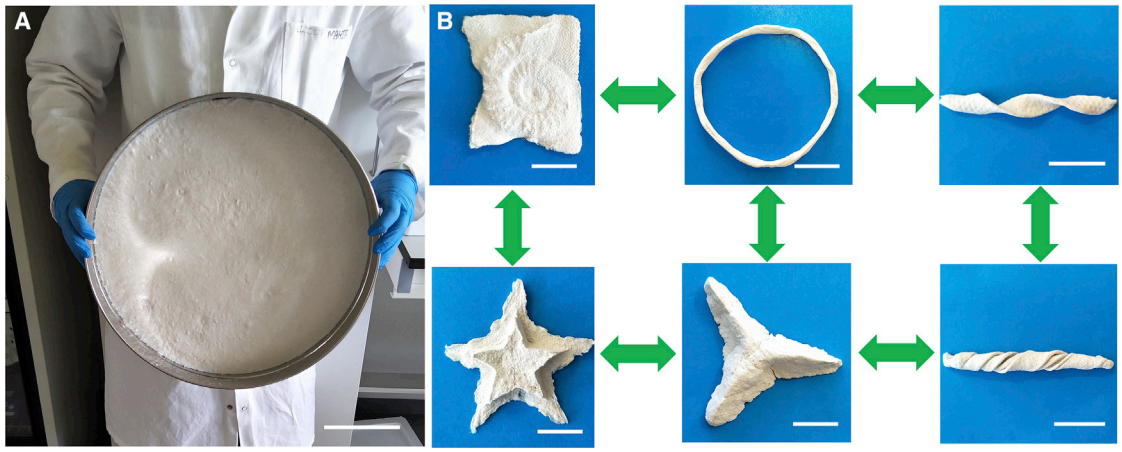

Figure 3. Recyclability of the biomineralized BC composites

(A) A 30-cm diameter biomineralized BC object (Ca^{2+}:Mg^{2+} 1:4), showing the possibility for mass production of the biomineralized BC. Scale bar, 10 cm.

(B) Biomineralized BC composites (Ca^{2+}: Mg^{2+} 1: 4) produced in a variety of shapes. The shape and size of the resulting material was tunable based on the shape of the mold. All of these shapes were fabricated from the same piece of material that was repeatedly remolded into different shapes. Scale bar, 2 cm.

Mechanical properties of biomineralized BC composites

Inspired by nacre, which is a natural $CaCO_3$ material possessing high toughness values due to its special layered "bricks and mortar" structure,[4] we hypothesized that the layered crystal-containing structure of our biomineralized BC composites likely plays a role in their mechanical properties.[18,19,22] The mechanical properties were therefore assessed with tensile testing (Figure 4). Specifically, we investigated the elongation at break and tensile strength values of the biomineralized BC composites, which are the two primary factors contributing to the final toughness values of a material.[4] Compared to pure BC, the elongation at break of biomineralized BC is significantly higher ($p < 0.01$) (Figure 4A). For samples produced with different Ca^{2+} content in the bacterial biomineralization medium ranging from 2.5 to 20 mM, the elongation at break varied from 8.0% $\pm$ 0.4% (pure BC) to 44.4% $\pm$ 1.8% (2.5 mM Ca^{2+}), 56.6% $\pm$ 0.4% (5.0 mM Ca^{2+}), then reaching its highest value (73.0% $\pm$ 1.1%) for samples with 10 mM Ca^{2+} in the bacterial biomineralization medium (Figure 4A), and finally decreasing to 17.9% $\pm$ 1.1% (20.0 mM Ca^{2+}). Since the elongation at break is an important factor contributing to a material's toughness, 10 mM was selected as the optimal Ca^{2+} concentration in the bacterial biomineralization medium to maximize toughness.

However, when Ca^{2+} content increased from 2.5 to 20 mM in the biomineralization medium, the ultimate tensile strength dropped significantly ($p < 0.01$), from 82.4 $\pm$ 0.6 MPa (pure BC) to 49.7 $\pm$ 1.4 MPa (2.5 mM Ca^{2+}), 29.3 $\pm$ 0.9 MPa (5.0 mM Ca^{2+}), 15.5 $\pm$ 0.4 MPa (10.0 mM Ca^{2+}), and 11.4 $\pm$ 0.1 MPa (20.0 mM Ca^{2+}) (Figure 4A). This reduction in tensile strength is likely due to the higher volume fraction of $CaCO_3$ crystals, which occupy the majority of the composite's volume and increase the brittleness of the material, decreasing its strength.

Since the addition of PGA and Mg^{2+} into the biomineralization medium reduced the crystal size (Figure 2), we assessed any resultant effect on the mechanical properties via tensile testing. With a Ca^{2+} and Mg^{2+} molar ratio of 1:4, the material showed enhanced tensile strength (47.2 $\pm$ 5.2 MPa; Figures 4B and 4C; Table S1) while displaying a high elongation at break (79.1% $\pm$ 2.8%). The biomineralized BC composites

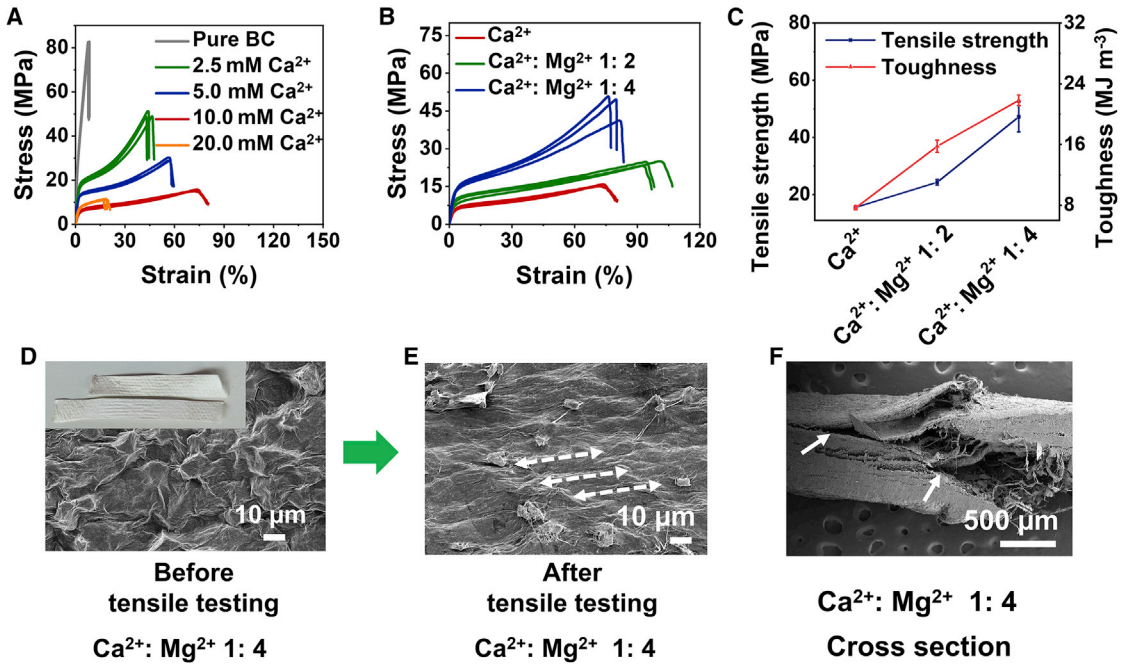

Figure 4. Mechanical properties of the biomineralized BC composites

(A) Tensile stress-strain curves of biomineralized BC with different Ca^{2+} content in the biomineralization medium.

(B and C) Tensile stress-strain curves (B), (C) tensile strength, and toughness values of biomineralized BC with and without Mg^{2+} ions in the biomineralization medium. Data are represented as means ± SDs.

(D and E) Optical and SEM images of the surface morphology of the biomineralized BC composite with Ca^{2+}: Mg^{2+} ratio of 1: 4 (D) before and (E) after tensile testing. Arrows represent stretched sample wrinkles after the application of load.

(F) SEM images of the cross-section of the biomineralized BC composite with Ca^{2+}:Mg^{2+} ratio of 1:4 after tensile testing. Arrows indicate delamination in the specimen.

All of the samples in this figure were made with PGA.

(Ca^{2+}:Mg^{2+} 1:4) showed a sharp increase in tensile strength before breaking (Figure 4B) in the final region of the stress-strain curve (strain hardening), as would be expected from the breakage of the numerous crystal-fiber connections (Figure S5). Because of this simultaneous increase in tensile strength and elongation at break, the toughness of the Mg^{2+}-containing biomineralized BC composite (Ca^{2+}:Mg^{2+} 1:4) was as high as 21.8 ± 0.7 MJ m^{-3} (Figure 4C; Table S1), which was 283% of the value for the sample without Mg^{2+} (7.7 ± 0.3 MJ m^{-3}) and 545% of the value for pure BC (4.0 ± 0.2 MJ m^{-3}). This increase in tensile strength and toughness correlates with the reduced crystal size, and thus with an increase in crystal density. In these composites, more entanglements would be present between $CaCO_3$ crystals and BC fibers (Figure 4D); thus, more energy would be needed to break the specimen. PGA may also help in improving toughness, since it can act as a viscoelastic glue in composite materials.[17] We therefore compared elongation at break values of biomineralized BC composites with and without PGA (produced with 10 mM Ca^{2+}) and found that the samples with PGA showed an elongation at break of 73.0% ± 1.1% (Figure 4A), which is higher compared to samples without PGA (59.4% ± 7.2%; Figure S6).

To further understand the mechanisms leading to such high toughness, both optical and SEM images of the biomineralized BC composites (Ca^{2+}:Mg^{2+} 1:4) before and after tensile testing were obtained. Unlike pure BC, the biomineralized BC composites were not fully broken after tensile testing but showed a marked increase in length (Figure 4D), also reflected in the high elongation at break. SEM results (Figures 4D and 4E) showed that the wrinkled surfaces before testing (Figure 4D, SEM image) of the biomineralized

BC composite specimens (Ca^{2+}:Mg^{2+} 1:4) became elongated (Figure 4E), which can explain the high elongation at break values. Meanwhile, delamination where layers separate from one another (Figure 4F, white arrows) and breakage of fiber-crystal entanglements (Figure 4F) occurred during failure under tension.

We also tested how well our biomineralized BC composites could resist compression. When a 100-kN force was applied to compress the biomineralized BC composites (Ca^{2+}:Mg^{2+} 1:4), the specimen became denser, with a reduction in thickness from 10 to 3.7 mm after compression (Figures S7A and S7B). Compression tests showed that our biomineralized BC composites were extremely compressible (Figure S7), not breaking even under a compression force as high as 100 kN. To elucidate the origin of such high compressibility, the surface (Figure S7C) and cross-section morphology (Figure S7D) of the compressed specimens (Ca^{2+}:Mg^{2+} 1:4) were imaged. A high density of micro-cracks (Figure S7C) was observed on the surface of the compressed specimens, while the layered cross-section morphology (Figure S7D) remained intact. These micro-cracks may allow the material to absorb the energy from the applied compression force, resulting in the compressible nature of the biomineralized BC composites, which may protect against extreme compression forces.

Since our material was highly compressible, we considered using compression as an additional (optional) processing step in the material fabrication. To test the influence of compression on the mechanical properties of the materials, tensile tests were carried out on the materials after being compressed with 100 kN of force (Figure S8). The compressed specimens showed an increase in ultimate tensile strength and a decrease in elongation at break compared with the noncompressed specimens (Table S1). The decrease in elongation at break could be due to the reduced surface roughness from the compression procedure (Figure S7C). However, compared to pure BC (elongation at break: 6.7% $\pm$ 1.3%; Table S1), the compressed biomineralized BC composites still showed relatively high values for elongation at break (>45%), which may be attributable to the intact layered structure.

The hardness (Figure 5A) and toughness of the materials were assessed before and after compression. In nonmineralized BC samples, the hardness values of the pure air-dried BC film remained similar before (179.5 $\pm$ 23.1 MPa) and after (182.7 $\pm$ 13.0 MPa) compressing. The biomineralized composite samples had hardness values up to >3 times lower than that of pure BC, with 49.3 $\pm$ 19.7 MPa (only Ca^{2+}), 61.2 $\pm$ 18.7 MPa (Ca^{2+}:Mg^{2+} 1:2), and 94.7 $\pm$ 9.1 MPa (Ca^{2+}:Mg^{2+} 1:4). Nevertheless, after being pressed with a 100-kN compression force, the hardness values increased significantly ($p < 0.01$) to 208.0 $\pm$ 36.2 MPa (only Ca^{2+}), 197.9 $\pm$ 9.1 MPa (Ca^{2+}:Mg^{2+} 1:2), and 251.1 $\pm$ 55.2 MPa (Ca^{2+}:Mg^{2+} 1:4), and became even higher than that of pure BC (182.7 $\pm$ 13.0 MPa). Optical microscope images of the biomineralized composites (Ca^{2+}:Mg^{2+} 1:4) after hardness testing (Figures 5B and 5C) showed that the indentation diameter for the compressed sample was smaller than the noncompressed specimen, consistent with an increase in hardness after compression.[46] This increase in hardness values indicates that we can tune the hardness of biomineralized BC by compression. Notably, the compressed samples retained almost the same toughness values (Table S1) compared with their noncompressed counterparts (Figure S8; Table S1).

To evaluate the impact resistance of the biomineralized BC composites, we used a dropping tower (Figure 5D). A mass of 1.6 kg was lifted to 1.5 m and released to hit the tested material with a speed of 5.0 m s^{-1} upon contacting the material. To test whether the specific mineralization method had an influence on the composite toughness, a control sample containing the same BC and Ca^{2+} concentrations in the

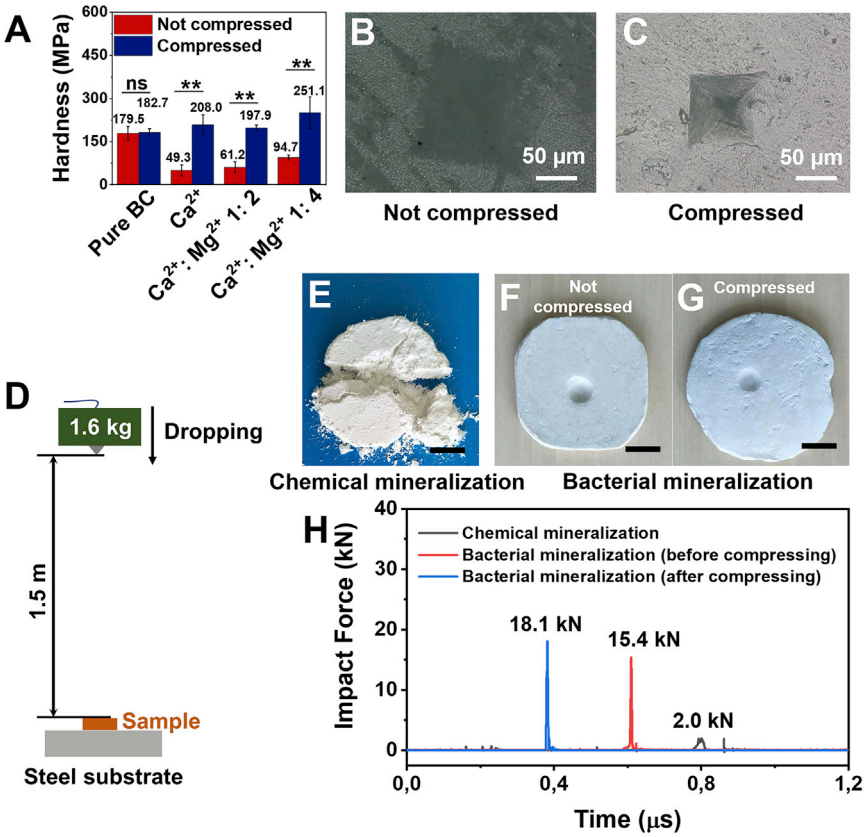

Figure 5. Hardness and impact resistance tests of the biomineralized BC composites

(A) Hardness values for pure BC and biomineralized BC composites before and after compression. Data are represented as means ± SDs.

(B and C) Optical microscope images of the biomineralized BC composite after hardness testing (Ca^{2+}:Mg^{2+} 1:4) (B) without and (C) with compression. **p < 0.01, significant; ns, not significant. Error bars represent SDs.

(D–G) The impact dropping tower (D) and (E–G) the samples after impact resistance testing. The sample thickness in (E)–(G) is 8 mm. Scale bar, 2 cm.

(H) The corresponding force-time curves during the impact resistance testing. All of the samples in this figure were made with PGA.

mineralization medium was prepared by traditional chemical mineralization in which $CaCl_2$ was reacted with Na_2CO_3 in a BC[23] slurry while stirring. Impact resistance testing of this sample resulted in a sharp, brittle disintegration (Figure 5E), while the biomineralized BC composite (Ca^{2+}:Mg^{2+} 1:4) with the same thickness (8 mm thick) was not broken (Figure 5F), showing that the biomineralized BC composite exhibited higher impact resistance than the chemically mineralized sample. The biomineralized BC composite (Ca^{2+}:Mg^{2+} 1:4) after compression was also tested by the impact resistance experiment (Figure 5G) and showed no observable breakage, also demonstrating higher impact resistance than the chemically mineralized sample. The force-time curves (Figure 5H) from the impact resistance testing indicated that both the noncompressed and compressed biomineralized BC composites (Ca^{2+}:Mg^{2+} 1:4) showed high peak impact resistance force values (18.1 kN, 15.4 kN), which is 7–9 times higher than the chemically mineralized sample (2 kN). The higher impact resistance of biomineralized BC can be attributed to its higher toughness (Table S1).

Since the bacterial biomineralized BC slurry was easily molded into different complex shapes and thicknesses (Figures 3B, 6A, and 6B) by simply fitting the slurry into a

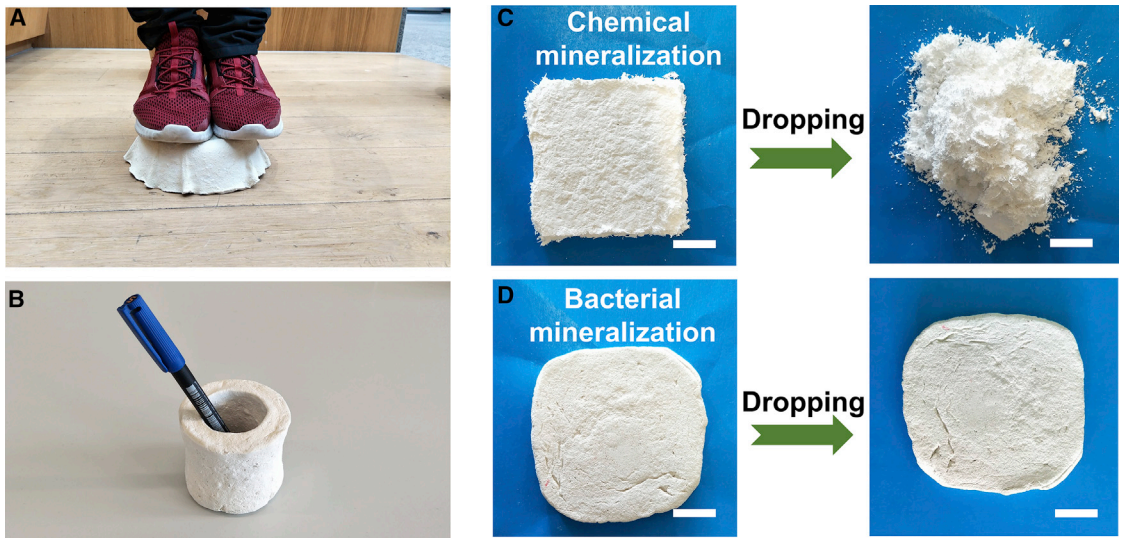

Figure 6. Examples for the applications of the biomineralized BC composites

(A and B) Biomineralized BC composites (Ca^{2+}:Mg^{2+} 1:4) molded into (A) a stool shape and (B) a cup.

(C and D) Composites produced with the (C) chemical method and (D) bacterial biomineralization method before (left) and after (right) dropping from a 10-m height 3 consecutive times. All of the samples in this figure were made with PGA. Scale bars correspond to 2 cm.

mold shape, we fabricated a stool and a cup. Such molded composite materials could withstand, as an example, a 70-kg person standing on it (hollow stool; Figure 6A), or be dropped from a >10-m height multiple times without any visible breakage (solid shape of 8 mm thickness; Figure 6D; Video S1). However, the chemically mineralized sample disintegrated into pieces after dropping 3 times from a height of 10 m (Figure 6C). The chemically mineralized BC composites could be broken easily by hand because they are vulnerable to far weaker forces than the large forces during impact tests. To assess the cause of this reduced impact resistance, we compared the structure of the biologically mineralized and the chemically mineralized samples. Two chemical mineralization methods were used here, either based on the reaction of $CaCl_2$ with Na_2CO_3[23] in a BC suspension (as for previous samples) or using gas diffusion.[47] Surprisingly, these two chemical approaches to form mineralized BC composites did not produce materials that demonstrate a layered structure (Figure S9A and 9B). The SEM images showed aggregated BC phases (Figure S9A, white arrows), separated by large clusters of $CaCO_3$, in contrast to the finely layered structure obtained via bacterial biomineralization (Figure 2), confirming the importance of the layers to obtain favorable mechanical properties, as also shown for nacre[4,29] and nacre-mimicking composites.[10,20] In biomineralized BC, the BC fibers were found to connect in between the layers to form fiber bridges (Figure S2) and to physically wrap around $CaCO_3$ crystals (Figure S5). These crystal-fiber entanglements may be the cause of the vastly different self-assembly behavior observed between the chemical and bacterial mineralization approaches.

To assess the fire-resistance properties of the biomineralized BC composites, specimens were exposed to the outer cone of the flame of a Bunsen burner. A pure organic filtrated BC sample, fabricated following the same procedure as biomineralized BC, without the addition of *S. pasteurii* bacteria, was used as a control. This control sample caught on fire immediately upon contact with the flame (Figure S10A), while the biomineralized BC resisted fire when exposed to a flame for 1 min (Figure S10B).

Since our biomineralized BC composite could be remolded into new shapes, we also tested the mechanical properties (Figure S11; Table S1) of the remolded samples

Table 1. Mechanical properties of biomineralized BC composites and other high-performance structural materials

Samples	Tensile strength (MPa)	Elongation at break (%)	Toughness (MJ m^{-3})	Hardness (MPa)	References
Ca^{2+}:Mg^{2+} 1:4 and PGA	47.2 ± 5.2	79.1 ± 2.8	21.8 ± 0.7	94.7 ± 9.1	This work
Ca^{2+}:Mg^{2+} 1:4 and PGA, compressed	50.6 ± 1.9	54.0 ± 11.1	21.3 ± 4.2	251.1 ± 55.2	This work
Pure BC	148.1 ± 13.4	4.5 ± 0.1	4.9 ± 0.8	–	[15]
Natural nacre	60–70	<1	0.2–2	950	[29,52]
Biomineralized BC	–	–	–	370	[24]
Cellulose nanofiber nacre	60–133	1–6	0.5–3	200–500	[53]
Gelatin-$CaCO_3$ nacre	30–97	3.1–12.5	–	–	[21]
Matrix-directed mineralized nacre	16–20	0.09–0.12	–	1,650	[18]
Biomineralized cross-lamella nacre	43.6 ± 4.5	<1	0.3 ± 0.7	–	[48]
ABS plastic	30–43	10–50	0.14–2.73	835	[54–56]

ABS, acrylonitrile butadiene styrene; BC, bacterial cellulose; PGA, poly(γ-glutamic acid).

(Ca^{2+}:Mg^{2+} 1:4). The tensile strength and toughness values of the remolded biomineralized BC composites did not significantly differ in comparison with their original counterparts.

DISCUSSION

We produce biomineralized BC composites with high and tunable toughness and stiffness via a combination of an environmentally friendly bacterial biomineralization procedure and an evaporation-induced self-assembly process. Our layered bacterially produced composites show a toughness (21.8 ± 0.7 MJ m^{-3}) over 5-fold higher than that of BC (4.0 ± 0.2 MJ m^{-3}). The mechanical properties of this material are tunable by adjusting the biomineralization components and post-processing method, where toughness values could be improved from 7.7 ± 0.3 MJ m^{-3} to 21.8 ± 0.7 MJ m^{-3} by adding Mg^{2+}, and hardness values could be improved from 94.7 ± 9.1 MPa to 251.1 ± 55.2 MPa by compressing.

The most commonly used type of method to fabricate layered structures containing $CaCO_3$ is layer-by-layer mineralization.[17,20,22] However, such methods are time-consuming and labor intensive and are challenging to apply for large-scale material production. A previous approach applying direct mineralization of a bulk substrate requires multiple mineralization cycles,[24] and only a limited mineral content is achievable, with most of the crystals attached only onto the surface of the substrate. To overcome this challenge, an external force has previously been used to push the mineralization solution into a pre-designed matrix,[18] to reach a mineral content similar to natural nacre. While this material possesses excellent toughness, such a fabrication approach is more technically difficult and produces lower tensile strength (38 MPa) and elongation at break (0.13%) compared to the material produced here. More recently, a $CaCO_3$-based mineralized synthetic nacre was prepared with a gas diffusion method,[48] creating in a mineral-interlocking microstructure to improve the mechanical properties. This material has a tensile strength (43.6 MPa) close to that of our material (50.6 MPa), but a significantly smaller elongation at break (0.9% versus 54.0%). Overall, our biomineralized BC composites show competitive strength and toughness values compared to most biomineralized synthetic nacre as well as to other natural or synthetic tough materials, including commercial acrylonitrile butadiene styrene (ABS) plastic (Table 1).

In addition to producing excellent mechanical properties, our fabrication procedure is based on easy processing compared to other materials with high impact-resistance properties, the fabrication of which is typically technically difficult[49] or energy consuming,[15] with limited shape control of the resultant materials. As the biomineralization process could be completed within 12 h and the biomineralized BC slurry could

self-assemble into a multi-layered structure by simply drying in the air, the whole fabrication procedure of our biomineralized BC composites is much faster compared to the month-long continual work of a layer-by-layer mineralization method[17] and the years-long biomineralization processes of natural nacre in nature.[29] Here, the fabrication procedure is fast, ecologically friendly, and readily scalable. Notably, this material could be recycled with a simple kitchen blender and a sieve, which is promising and convenient for daily-life applications. Due to these features, this fully biodegradable, highly tough material shows multiple promising applications in daily human life, including the production of furniture, cellphone holders, helmets, and protective garments.

EXPERIMENTAL PROCEDURES

Resource availability

Lead contact

Marie-Eve Aubin-Tam (email: m.e.aubin-tam@tudelft.nl).

Materials availability

This study did not generate new unique reagents.

Data and code availability

All experimental data, computational data, and code are available upon reasonable request to the lead contact author.

Materials

D(+)-glucose monohydrate and di-sodium hydrogen phosphate (≥99.0%) were obtained from Carl Roth GmbH. All of the other chemicals were purchased from Sigma-Aldrich.

Preparation of BC slurry

For cellulose production, *G. hansenii* (ATCC 53582) were grown statically at 30°C in Hestrin-Schramm (HS) medium (5 g L^{-1} tryptone, 5 g L^{-1} yeast extract, 2.7 g L^{-1} disodium hydrogen phosphate, 1.5 g L^{-1} citric acid, and 20 g L^{-1} glucose). The BC pellicle formed at the air-liquid interface was harvested after 15 days of incubation and boiled on a heating plate at 100°C with a 1 w/v% solution of sodium hydroxide for 10 min to kill the bacteria. The pellicle was then washed and immersed in distilled water several times to remove the impurities. The washing steps were repeated until the pellicles turned pure white.

For the BC slurry preparation, 120 mL water was mixed with 30 g wet BC pellicle, and the BC pellicle/water mixture was mechanically homogenized into a fibrous suspension with a kitchen blender for 5 min. The BC slurry was then autoclaved and stored at 4°C.

Preparation of bacterial PGA

Bacterial PGA is produced as previously reported.[17,50,51] Briefly, overnight cultures of *B. licheniformis* (NBRC12107, NBRC, Japan) grown in BL medium (10 g L^{-1} peptone, 2 g L^{-1} yeast extract, and 1 g L^{-1} $MgSO_4 \cdot H_2O$) were added at 1.5 v/v% to autoclaved PGA production medium (20 g L^{-1} L-glutamic acid, 13.6 g L^{-1} sodium citrate monobasic, 80 g L^{-1} glycerol, 7 g L^{-1} NH_4Cl, 0.5 g L^{-1} KH_2PO_4, 0.244 g L^{-1} $MgSO_4$, 0.04 g L^{-1} $FeCl_3 \cdot 6H_2O$, 0.15 g L^{-1} $CaCl_2 \cdot 2H_2O$, 0.1 g L^{-1} $MnSO_4 \cdot H_2O$, pH was adjusted to 7.5 with NaOH) and incubated at 30°C for 48 h at 180 rpm. After incubation, the viscous PGA solution was centrifuged at 8,200 × *g* for 15 min at 4°C to remove the bacteria. The polymer solution was diluted with twice the volume of ethanol. The precipitated PGA polymer was then dried at 50°C for 2 days.

Bacterially induced biomineralization

S. pasteurii bacteria (DSM-33, ATCC 11859, DSMZ, Germany) were inoculated into 50 mL SP2 medium (20 g L^{-1} yeast extract, 10 g L^{-1} NH_4Cl, 10 μM $NiCl_2$, pH was adjusted to 8.5 with NaOH) and incubated for 48 h at 28°C at 180 rpm. The bacterial solution was centrifuged at 1,500 × *g* for 15 min. The supernatant was removed, and the bacteria pellet was re-suspended with 25 mL fresh SP2 medium and 25 mL sterile 40 w/v% glycerol. The SP2 glycerol stocks were stored at −80°C for use.

The slurry mixture for biomineralization consisted of 400 mL L^{-1} BC slurry (120 g wet BC hydrogel), 20 g L^{-1} urea, 10 g L^{-1} tryptone, 5 g L^{-1} yeast extract, 10 g L^{-1} NH_4Cl, 1 mL L^{-1} of SP2 glycerol stock, 1 g L^{-1} PGA, and $CaCl_2 \cdot 2H_2O$/$MgCl_2 \cdot 6H_2O$ solution. The overall concentrations of Ca^{2+}/Mg^{2+} in the medium are listed here for each condition tested: 2.5 mM only Ca^{2+}: 2.5 mM $CaCl_2 \cdot 2H_2O$; 5.0 mM only Ca^{2+}: 5 mM $CaCl_2 \cdot 2H_2O$; 10.0 mM only Ca^{2+}: 10 mM $CaCl_2 \cdot 2H_2O$; 20.0 mM only Ca^{2+}: 20 mM $CaCl_2 \cdot 2H_2O$; 1:2 Ca^{2+}:Mg^{2+}: 3.33 mM $CaCl_2 \cdot 2H_2O$ and 6.67 mM $MgCl_2 \cdot 6H_2O$; 1:4 Ca^{2+}:Mg^{2+}: 2 mM $CaCl_2 \cdot 2H_2O$ and 8 mM $MgCl_2 \cdot 6H_2O$. The slurry containing bacteria was incubated statically at 28°C for 12 h for biomineralization. There was no difference in pH change during $CaCO_3$ precipitation with and without addition of PGA, which was used to adjust the crystal morphology.

Self-assembly of bacterial composites

After biomineralization, the slurry was boiled for 10 min for sterilization, and the liquid medium was removed by filtering the slurry with a kitchen sieve and rinsing with distilled water. The condensed mud-like slurry was then molded into various shapes and sizes. Finally, the material was dried for 2 days at room temperature to form the resulted composites.

For the control sample of pure filtrated BC, all of the formulations and post-treatment methods were similar to those for the biomineralized BC composites (10 mM Ca^{2+} concentration in the biomineralization medium), except that no *S. pasteurii* bacteria were added into the biomineralization medium.

For the control samples for impact resistance testing, a chemical mineralization method was used. Briefly, 10 mM Na_2CO_3 was added into the 400 mL L^{-1} BC slurry (120 g wet BC hydrogel) with 10 mM $CaCl_2 \cdot 2H_2O$ and 1 g L^{-1} PGA solution while stirring. The resultant BC-$CaCO_3$ mixture was vacuum filtrated and dried in the fume hood for 2 days at room temperature.

For the gas diffusion method,[47] 10 g BC bulk hydrogel or 10 g blended BC suspension was placed into a Petri dish and mixed with 20 mL 5 M $CaCl_2 \cdot 2H_2O$. The mixture was then put into a sealed desiccator containing a beaker filled with 100 g $(NH_4)_2CO_3$ powder. The mineralization was carried out for 7 days.

SEM

The sample morphology was observed with an SEM (JEOL JSM 6010 LA). Samples were sputter coated with gold-palladium at 20 mA for 60 s. The imaging was carried out under the secondary electron imaging (SEI) mode at 5–15 kV in vacuum. Crystal diameters and layer thickness values were measured with the ImageJ software from SEM images taken in >100 different regions within the samples.

Tensile testing

The tensile properties were measured using a Zwick LF7M10 universal testing machine with a 10-kN load cell, the grip distance was 10 mm, and the samples were

tested with a loading rate of 2 mm min^{-1}. At least three specimens per group were measured for the data presented. The toughness of the biomineralized BC composites was calculated according to Equation 1:

$$U = \int_0^{\varepsilon_f} \sigma \, d\varepsilon \qquad \text{(Equation 1)}$$

where U is the energy per volume absorbed, σ is the stress, ε is the strain, and ε_f is the elongation at break.

Compression testing

The compression testing was carried out using a Zwick LF7M19 universal testing machine with a 250-kN load cell. The samples were compressed to 100 kN with a loading rate of 5 mm min^{-1}.

Hardness testing

Specimens for micro-indentation were embedded into an epoxy resin (Epofix Cold-Setting Embedding Resin, volume ratio of epoxy and hardener was 15:2) and polished with decreasing grades of polishing papers (SiC foils #1200, #2000, and #4000, Struers) to obtain a mirror surface. Vickers hardness measurements were performed under a test force of 0.2 kgf (further denoted as HV0.2) using an Automatic MicroHardness Tester (Struers Dura Scan 70). The embedded samples were indented by a standard Vickers indenter (L 5 mm, Ø 6 mm), with at least 8 indents performed for each sample. An optical microscope (OM, VH-Z250R, KEYENCE, USA) was used to image the surface morphology after the hardness measurements.

Impact resistance testing

The samples were placed onto a flat stainless-steel table. Then, a dropping tower (1.6 kg) with a steel tip (tip diameter = 5 mm) was lifted to the maximum height (1.5 m) and released. The maximum speed was 5.0 m s^{-1}. At least three specimens were measured for each sample type.

Dropping experiment

The materials were brought to a height of >10 m inside a building and dropped to the ground floor. Each sample was dropped three times. Samples were photographed before and after dropping.

TGA

Thermal properties were measured using a TGA machine (Mettler Toledo) at 30°C–1,000°C, with a heating rate of 10°C min^{-1} in an air atmosphere. At 600°C, the mass of pure BC reached 0%, while the mass of $CaCO_3$ remained at 100% of its initial value. Therefore, the $CaCO_3$ content in the final composite can be represented from the mass ratio values at 600°C.

XRD

XRD was carried out with a Bruker D8 Advance diffractometer Bragg-Brentano geometry and Lynxeye position-sensitive detector, Cu K_α radiation. The parameters used were the following: divergence slit V12, scatter screen height 5 mm, 45 kV 40 mA, sample spinning, and detector settings: LL 0.11 and W 0.14. Measurements were carried out with a coupled θ–2θ scan of 10°–110°, step size of 0.021°, and a counting time of 1 s per step. Data evaluation was carried out with Bruker software DiffracSuite.EVA versus 4.3.

Fire-resistance testing

The specimens were exposed to the outer cone flame of a Bunsen burner.

Statistical analysis

Statistical analysis was performed on https://astatsa.com/. The groups were compared with one-way (single-factor) ANOVA with post hoc Tukey's HSD (honest significant difference) tests. $p < 0.05$, significant.

SUPPLEMENTAL INFORMATION

Supplemental information can be found online at https://doi.org/10.1016/j.xcrp.2021.100464.

ACKNOWLEDGMENTS

The authors thank Berthil Grashof for tensile testing, Dave Ruijtenbeek for compression testing, Misja Huizinga for impact resistance testing, Jianing Zhu for hardness testing, Jiahui Dong for the optical microscope images after hardness testing, Bart van der Linden for the TGA measurements, and Roland Kieffer and Ramon van der Valk for lab support. The authors acknowledge Jeroen Methorst, Heleen Oude Nijhuis, Erick Espindola Perez, and Melina Dekker for earlier strategies to process bacterial cellulose. The authors thank Ward Groutars and Elvin Karana for useful discussions. K.Y. is supported financially by the China Scholarship Council (CSC no. 201706630001). S.B. is funded by the Air Force Office of Scientific Research, Asian Office of Aerospace Research and Development (grant no. FA2386-18-1-4059).

AUTHOR CONTRIBUTIONS

M.-E.A.-T., A.S.M., K.Y., and D.T.S. designed the project. K.Y. carried out the material fabrication procedure and performed the SEM, tensile, compression, hardness, TGA, XRD, optical microscope, and impact-resistance testing experiments. E.M.S., K.Y., and M.-E.A.-T. discussed the mechanical testing and the biomineralization experiments. S.B. and K.Y. performed the fire-resistance and dropping experiments, and captured the optical images. D.T.S., K.Y., S.B., A.S.M., and M.-E.A.-T. developed the BC growing and washing procedure. All of the authors wrote the manuscript.

DECLARATION OF INTERESTS

A patent application has been filed with Kui Yu and Marie-Eve Aubin-Tam as the authors and "Biomineralized Cellulose Material" as the title.

Received: December 7, 2020
Revised: April 19, 2021
Accepted: May 19, 2021
Published: June 10, 2021

REFERENCES

1. Mohanty, A.K., Vivekanandhan, S., Pin, J.-M., and Misra, M. (2018). Composites from renewable and sustainable resources: challenges and innovations. Science *362*, 536–542.

2. Zhang, F., Lan, X., Peng, H., Hu, X., and Zhao, Q. (2020). A "trojan horse" camouflage strategy for high-performance cellulose paper and separators. Adv. Funct. Mater. *30*, 2002169.

3. Zhu, Y., Romain, C., and Williams, C.K. (2016). Sustainable polymers from renewable resources. Nature *540*, 354–362.

4. Wegst, U.G., Bai, H., Saiz, E., Tomsia, A.P., and Ritchie, R.O. (2015). Bioinspired structural materials. Nat. Mater. *14*, 23–36.

5. Tu, H., Zhu, M., Duan, B., and Zhang, L. (2020). Recent progress in high-strength and robust regenerated cellulose materials. Adv. Mater. https://doi.org/10.1002/adma.202000682.

6. Khakalo, A., Tanaka, A., Korpela, A., and Orelma, H. (2020). Delignification and ionic liquid treatment of wood toward multifunctional high-performance structural materials. ACS Appl. Mater. Interfaces *12*, 23532–23542.

7. Ma, L., Bi, Z., Xue, Y., Zhang, W., Huang, Q., Zhang, L., and Huang, Y. (2020). Bacterial cellulose: an encouraging eco-friendly nano-candidate for energy storage and energy conversion. J. Mater. Chem. A Mater. Energy Sustain. *8*, 5812–5842.

8. Wu, Z.Y., Liang, H.W., Chen, L.F., Hu, B.C., and Yu, S.H. (2016). Bacterial cellulose: a robust platform for design of three dimensional carbon-based functional nanomaterials. Acc. Chem. Res. *49*, 96–105.

9. Yu, K., Balasubramanian, S., Pahlavani, H., Mirzaali, M.J., Zadpoor, A.A., and Aubin-Tam, M.E. (2020). Spiral honeycomb microstructured

bacterial cellulose for increased strength and toughness. ACS Appl. Mater. Interfaces *12*, 50748–50755.

10. Guan, Q.-F., Yang, H.-B., Han, Z.-M., Zhou, L.-C., Zhu, Y.-B., Ling, Z.-C., Jiang, H.-B., Wang, P.-F., Ma, T., Wu, H.-A., and Yu, S.H. (2020). Lightweight, tough, and sustainable cellulose nanofiber-derived bulk structural materials with low thermal expansion coefficient. Sci. Adv. *6*, eaaz1114.

11. Ritchie, R.O. (2011). The conflicts between strength and toughness. Nat. Mater. *10*, 817–822.

12. Wang, S., Jiang, F., Xu, X., Kuang, Y., Fu, K., Hitz, E., and Hu, L. (2017). Super-strong, super-stiff macrofibers with aligned, long bacterial cellulose nanofibers. Adv. Mater. *29*, 1702498.

13. Yao, J., Chen, S., Chen, Y., Wang, B., Pei, Q., and Wang, H. (2017). Macrofibers with high mechanical performance based on aligned bacterial cellulose nanofibers. ACS Appl. Mater. Interfaces *9*, 20330–20339.

14. Yu, S.-H., Wu, H.-A., Liu, C., Wen, S.-M., Meng, Y.-F., Pan, Z., Chen, S.-M., Zhu, Y.-B., Cui, C., Zhao, R., et al. (2020). Bioinspired hierarchical helical nanocomposite macrofibers based on bacterial cellulose nanofibers. Natl. Sci. Rev. *7*, 73–83.

15. Wu, Z., Chen, S., Wu, R., Sheng, N., Zhang, M., Ji, P., and Wang, H. (2020). Top-down peeling bacterial cellulose to high strength ultrathin films and multifunctional fibers. Chem. Eng. J. *391*, 123527.

16. Rahman, M.M., and Netravali, A.N. (2016). Aligned bacterial cellulose arrays as "green" nanofibers for composite materials. ACS Macro Lett. *5*, 1070–1074.

17. Spiesz, E.M., Schmieden, D.T., Grande, A.M., Liang, K., Schwiedrzik, J., Natalio, F., Michler, J., Garcia, S.J., Aubin-Tam, M.-E., and Meyer, A.S. (2019). Bacterially produced, nacre-inspired composite materials. Small *15*, 1805312.

18. Mao, L.-B., Gao, H.-L., Yao, H.-B., Liu, L., Cölfen, H., Liu, G., Chen, S.-M., Li, S.-K., Yan, Y.-X., Liu, Y.-Y., and Yu, S.H. (2016). Synthetic nacre by predesigned matrix-directed mineralization. Science *354*, 107–110.

19. Chen, Y., Fu, J., Dang, B., Sun, Q., Li, H., and Zhai, T. (2020). Artificial wooden nacre: a high specific strength engineering material. ACS Nano *14*, 2036–2043.

20. Finnemore, A., Cunha, P., Shean, T., Vignolini, S., Guldin, S., Oyen, M., and Steiner, U. (2012). Biomimetic layer-by-layer assembly of artificial nacre. Nat. Commun. *3*, 966.

21. Li, X.Q., and Zeng, H.C. (2012). Calcium carbonate nanotablets: bridging artificial to natural nacre. Adv. Mater. *24*, 6277–6282.

22. Farhadi-Khouzani, M., Schütz, C., Durak, G.M., Fornell, J., Sort, J., Salazar-Alvarez, G., et al. (2017). A $CaCO_3$/nanocellulose-based bioinspired nacre-like material. J. Mater. Chem. A Mater. Energy Sustain. *5*, 16128–16133.

23. Liu, X., Zhou, Y., and Pei, C. (2018). Mimetic biomineralization matrix using bacterial cellulose hydrogel and egg white to prepare various morphologies of $caco_3$. CrystEngComm *20*, 4536–4540.

24. Cheng, Z., Ye, Z., Natan, A., Ma, Y., Li, H., Chen, Y., Wan, L., Aparicio, C., and Zhu, H. (2019). Bone-inspired mineralization with highly aligned cellulose nanofibers as template. ACS Appl. Mater. Interfaces *11*, 42486–42495.

25. Phillips, A.J., Gerlach, R., Lauchnor, E., Mitchell, A.C., Cunningham, A.B., and Spangler, L. (2013). Engineered applications of ureolytic biomineralization: a review. Biofouling *29*, 715–733.

26. Heveran, C.M., Liang, L., Nagarajan, A., Hubler, M.H., Gill, R., Cameron, J.C., Cook, S.M., and Srubar, W.V., 3rd (2019). Engineered ureolytic microorganisms can tailor the morphology and nanomechanical properties of microbial-precipitated calcium carbonate. Sci. Rep. *9*, 14721.

27. Heveran, C.M., Williams, S.L., Qiu, J., Artier, J., Hubler, M.H., Cook, S.M., Cameron, J.C., and Srubar, W.V. (2020). Biomineralization and successive regeneration of engineered living building materials. Matter *2*, 481–494.

28. Yu, Y., Yan, F., Chen, Y., Jin, C., Guo, J.H., and Chai, Y. (2016). Poly-γ-glutamic acids contribute to biofilm formation and plant root colonization in selected environmental isolates of Bacillus subtilis. Front. Microbiol. *7*, 1811.

29. Barthelat, F. (2010). Nacre from mollusk shells: a model for high-performance structural materials. Bioinspir. Biomim. *5*, 035001.

30. Breschi, L., Maravic, T., Cunha, S.R., Comba, A., Cadenaro, M., Tjäderhane, L., Pashley, D.H., Tay, F.R., and Mazzoni, A. (2018). Dentin bonding systems: from dentin collagen structure to bond preservation and clinical applications. Dent. Mater. *34*, 78–96.

31. Ghosh, T., Bhaduri, S., Montemagno, C., and Kumar, A. (2019). Sporosarcina pasteurii can form nanoscale calcium carbonate crystals on cell surface. PLoS ONE *14*, e0210339.

32. Qin, W., Wang, C.Y., Ma, Y.X., Shen, M.J., Li, J., Jiao, K., Tay, F.R., and Niu, L.N. (2020). Microbe-mediated extracellular and intracellular mineralization: environmental, industrial, and biotechnological applications. Adv. Mater. *32*, e1907833.

33. Florea, M., Reeve, B., Abbott, J., Freemont, P.S., and Ellis, T. (2016). Genome sequence and plasmid transformation of the model high-yield bacterial cellulose producer Gluconacetobacter hansenii ATCC 53582. Sci. Rep. *6*, 23635.

34. Li, Q., Gao, R., Wang, L., Xu, M., Yuan, Y., Ma, L., Wan, Z., and Yang, X. (2020). Nanocomposites of bacterial cellulose nanofibrils and zein nanoparticles for food packaging. ACS Appl. Nano Mater. *3*, 2899–2910.

35. Santmarti, A., Zhang, H., Lappalainen, T., and Lee, K.-Y. (2020). Cellulose nanocomposites reinforced with bacterial cellulose sheets prepared from pristine and disintegrated pellicle. Compos. Part A *130*, 105766.

36. Ghayoor, H., Hoa, S.V., and Marsden, C.C. (2018). A micromechanical study of stress concentrations in composites. Compos. Part B *132*, 115–124.

37. Mi, D., Xia, C., Jin, M., Wang, F., Shen, K., and Zhang, J. (2016). Quantification of the effect of shish-kebab structure on the mechanical properties of polypropylene samples by controlling shear layer thickness. Macromolecules *49*, 4571–4578.

38. Tom, S., Jin, H.E., Heo, K., and Lee, S.W. (2016). Engineered phage films as scaffolds for $CaCO_3$ biomineralization. Nanoscale *8*, 15696–15701.

39. Llauro, M.-F., Loiseau, J., Boisson, F., Delolme, F., Ladavière, C., and Claverie, J. (2004). Unexpected end-groups of poly(acrylic acid) prepared by raft polymerization. J. Polym. Sci. A Polym. Chem. *42*, 5439–5462.

40. Moradali, M.F., and Rehm, B.H.A. (2020). Bacterial biopolymers: from pathogenesis to advanced materials. Nat. Rev. Microbiol. *18*, 195–210.

41. Ogunleye, A., Bhat, A., Irorere, V.U., Hill, D., Williams, C., and Radecka, I. (2015). Poly-γ-glutamic acid: production, properties and applications. Microbiology (Reading) *161*, 1–17.

42. Arias, J.L., and Fernández, M.S. (2008). Polysaccharides and proteoglycans in calcium carbonate-based biomineralization. Chem. Rev. *108*, 4475–4482.

43. Davis, K.J., Dove, P.M., and De Yoreo, J.J. (2000). The role of Mg^{2+} as an impurity in calcite growth. Science *290*, 1134–1137.

44. Rahman, M.A., Halfar, J., and Shinjo, R. (2013). X-ray diffraction is a promising tool to characterize coral skeletons. Adv. Mater. Phys. Chem. *3*, 120–125.

45. Tsortos, A., and Nancollas, G.H. (2002). The role of polycarboxylic acids in calcium phosphate mineralization. J. Colloid Interface Sci. *250*, 159–167.

46. Shahdad, S.A., McCabe, J.F., Bull, S., Rusby, S., and Wassell, R.W. (2007). Hardness measured with traditional Vickers and Martens hardness methods. Dent. Mater. *23*, 1079–1085.

47. Xu, A.W., Antonietti, M., Cölfen, H., and Fang, Y.P. (2006). Uniform hexagonal plates of vaterite $caco_3$ mesocrystals formed by biomimetic mineralization. Adv. Funct. Mater. *16*, 903–908.

48. Raut, H.K., Schwartzman, A.F., Das, R., Liu, F., Wang, L., Ross, C.A., and Fernandez, J.G. (2020). Tough and strong: cross-lamella design imparts multifunctionality to biomimetic nacre. ACS Nano *14*, 9771–9779.

49. Yin, Z., Hannard, F., and Barthelat, F. (2019). Impact-resistant nacre-like transparent materials. Science *364*, 1260–1263.

50. Yu, K., and Aubin-Tam, M.-E. (2020). Bacterially grown cellulose/graphene oxide composites infused with γ-poly (glutamic acid) as biodegradable structural materials with enhanced toughness. ACS Appl. Nano Mater. *3*, 12055–12063.

51. Liang, K., Spiesz, E.M., Schmieden, D.T., Xu, A.W., Meyer, A.S., and Aubin-Tam, M.E. (2020). Bioproduced polymers self-assemble with graphene oxide into nanocomposite films with

enhanced mechanical performance. ACS Nano *14*, 14731–14739.

52. Kakisawa, H., and Sumitomo, T. (2012). The toughening mechanism of nacre and structural materials inspired by nacre. Sci. Technol. Adv. Mater. *12*, 064710.

53. Yan, Y.-X., Yao, H.-B., and Yu, S.-H. (2016). Nacre-like ternary hybrid films with enhanced mechanical properties by interlocked nanofiber design. Adv. Mater. Interfaces *3*, 1600296.

54. Bai, X., Isaac, D.H., and Smith, K. (2007). Reprocessing acrylonitrile–butadiene–styrene plastics: structure–property relationships. Polym. Eng. Sci. *47*, 120–130.

55. Mamaghani Shishavan, S., Azdast, T., and Rash Ahmadi, S. (2014). Investigation of the effect of nanoclay and processing parameters on the tensile strength and hardness of injection molded acrylonitrile butadiene styrene–organoclay nanocomposites. Mater. Des. *58*, 527–534.

56. Ching, E.C.Y., Poon, W.K.Y., Li, R.K.Y., and Mai, Y.-W. (2000). Effect of strain rate on the fracture toughness of some ductile polymers using the essential work of fracture (ewf) approach. Polym. Eng. Sci. *40*, 2558–2568.